Supplemental Information

Multidrug treatment with nelfinavir and cepharanthine against COVID-19

Hirofumi Ohashi[1,2,¶], Koichi Watashi[1,2,3,4*], Wakana Saso[1,5,6,¶], Kaho Shionoya[1,2], Shoya Iwanami[7], Takatsugu Hirokawa[8,9,10], Tsuyoshi Shirai[11], Shigehiko Kanaya[12], Yusuke Ito[7], Kwang Su Kim[7], Kazane Nishioka[1,2], Shuji Ando[13], Keisuke Ejima[14], Yoshiki Koizumi[15], Tomohiro Tanaka[16], Shin Aoki[16,17], Kouji Kuramochi[2], Tadaki Suzuki[18], Katsumi Maenaka[19], Tetsuro Matano[5,6], Masamichi Muramatsu[1], Masayuki Saijo[13], Kazuyuki Aihara[20], Shingo Iwami[4,7,21,22,23], Makoto Takeda[24], Jane A. McKeating[25], Takaji Wakita[1]

[1]Department of Virology II, National Institute of Infectious Diseases, Tokyo 162-8640, Japan,
[2]Department of Applied Biological Science, Tokyo University of Science, Noda 278-8510, Japan,
[3]Institute for Frontier Life and Medical Sciences, Kyoto University, Kyoto 606-8507, Japan,
[4]MIRAI, JST, Saitama 332-0012, Japan,
[5]The Institute of Medical Science, The University of Tokyo, Tokyo 108-8639, Japan,
[6]AIDS Research Center, National Institute of Infectious Diseases, Tokyo 162-8640, Japan,
[7]Department of Biology, Faculty of Sciences, Kyushu University, Fukuoka 812-8581, Japan,
[8]Cellular and Molecular Biotechnology Research Institute, National Institute of Advanced Industrial Science and Technology, Tokyo 135-0064, Japan,
[9]Division of Biomedical Science, Faculty of Medicine, University of Tsukuba, Tsukuba 305-8575, Japan,
[10]Transborder Medical Research Center, University of Tsukuba, Tsukuba 305-8575, Japan,
[11]Faculty of Bioscience, Nagahama Institute of Bio-Science and Technology, Nagahama 526-0829, Japan,
[12]Graduate School of Science and Technology, Nara Institute of Science and Technology, Ikoma 630-0192, Japan,
[13]Department of Virology I, National Institute of Infectious Diseases, Tokyo 162-8640, Japan,
[14]Department of Epidemiology and Biostatistics, Indiana University School of Public Health-Bloomington, IN 47405, USA,
[15]National Center for Global Health and Medicine, Tokyo162-8655, Japan,
[16]Faculty of Pharmaceutical Sciences, Tokyo University of Science, Noda 278-8510, Japan,
[17]Research Institute for Science and Technology, Tokyo University of Science, Noda 278-8510, Japan,
[18]Department of Pathology, National Institute of Infectious Diseases, Tokyo 162-8640, Japan,
[19]Faculty of Pharmaceutical Sciences, Hokkaido University, Sapporo 060-0812, Japan,
[20]International Research Center for Neurointelligence, The University of Tokyo Institutes for Advanced Study, The University of Tokyo, Tokyo 113-8654, Japan,
[21]Institute for the Advanced Study of Human Biology (ASHBi), Kyoto University, Kyoto 606-8501, Japan,
[22]NEXT-Ganken Program, Japanese Foundation for Cancer Research (JFCR), Tokyo 135-8550, Japan,
[23]Science Groove Inc., Fukuoka 810-0041, Japan,
[24]Department of Virology III, National Institute of Infectious Diseases, Tokyo 208-0011, Japan,
[25]Nuffield Department of Medicine, University of Oxford, Oxford OX3 7FZ, UK.

Supplementary Methods

Cell culture. VeroE6/TMPRSS2 cells [VeroE6 cells overexpressing transmembrane protease, serine 2 (TMPRSS2) (Matsuyama et al., 2020) were cultured in Dulbecco's modified Eagle's medium (DMEM; Life Technologies) supplemented with 10% fetal bovine serum (FBS; Cell Culture Bioscience), 10 units/mL penicillin, 10 mg/mL streptomycin, 10 mM HEPES (pH 7.4), and 1 mg/mL G418 (Nacalai) at 37˚C in 5% CO_2. During the infection assay, 10% FBS was replaced by 2% FBS and G418 removed.

Reagents. All the reagents were purchased from Selleck, Enzo Life Sciences, Cayman Chemical, Sigma, MedChemExpress, TCI or kindly donated by pharmaceutical companies (Abbvie, Alps Pharmaceutical, Asahi Kasei Pharma, Astellas Pharma, Bayer, Boehringer Ingelheim, Bristol-Myers Squibb, Chugai Pharmaceutical, Daiichi Sankyo, EA Pharma, Fujifilm Toyama Chemical, Japan Tobacco, Kakenshoyaku, Kissei Pharmaceutical, Kowa, Kyorin Pharmaceutical, Kyowa Pharmaceutical Industry, Maruho, Mitsubishi Tanabe Pharma, Mochida Pharmaceutical, Novartis, Sanofi, SBI Pharmaceuticals, Shionogi, Sumitomo Dainippon Pharma, Sun Pharma, Takeda Pharmaceutical, Teva Takeda Pharma). Note that throughout in this study we used the pharmaceutical preparation of Cepharanthine (kindly provided by Medisa Shinyaku Inc, a subsidiary of Sawai Pharmaceutical), which is a Stephania-derived alkaloid extract containing 19.5-33.5% Cepharanthine molecule as the major component.

Infection assay. SARS-CoV-2 was handled in a biosafety level 3 (BSL3). We used the SARS-CoV-2 Wk-521 strain, a clinical isolate from a COVID-19 patient, and obtained viral stocks by infecting VeroE6/TMPRSS2 cells (Matsuyama et al., 2020). Virus infectious titers were measured by inoculating cells with a 10-fold serial dilution of virus and cytopathology measured to calculate $TCID_{50}$/ml (Matsuyama et al., 2020). For the infection assay, VeroE6/TMPRSS2 cells were inoculated with virus at an MOI of 0.01 (Fig. 1 and 2B) or 0.001 (Fig. 2D and 3) for 1 h and unbound virus removed by washing. Cells were cultured for 24 h prior to measuring extracellular viral RNA or detecting viral encoded N protein, and cytopathic effects (CPE) after 48 h. Compounds were added during virus inoculation (1 h) and replenished after washing (24 or 48 h) except for time of addition assay.

For the time of addition assay, we added compounds with three different timings (Fig. 2A): (a) present during the 1 h virus inoculation step and maintained throughout the 24 h infection period (**whole life cycle**); (b) present during the 1 h virus inoculation step and for an additional 2 h and then removed (**entry**); or (c) added after the inoculation step and present for the remaining 22 h of infection (**post-entry**). Inhibitors of viral replication are expected to show antiviral activity in (a) and (c), but not (b), while entry inhibitors (e.g. chloroquine) reduce viral RNA in all three conditions (In c, addition of entry inhibitors after inoculation inhibits re-infection and thus decreases viral RNA) (Wang et al., 2020).

Quantification of viral RNA. Viral RNA was extracted with a QIAamp Viral RNA mini kit (QIAGEN) and quantified by real time RT-PCR analysis with a one-step qRT-PCR kit (THUNDERBIRD Probe One-step qRT-PCR kit, TOYOBO) using 5'- ACAGGTACGTTAATAGTTAATAGCGT-3' and 5'-

ATATTGCAGCAGTACGCACACA-3' as the primer set and a 5'-FAM-ACACTAGCCATCCTTACTGCGCTTCG-TAMRA-3' probe, as described (Corman et al., 2020). Detection limit of SARS-CoV-2 RNA in this study was 38 cycle as C_t cycle.

Detection of viral N protein. Viral protein expression was detected using a rabbit anti-SARS-CoV N antibody (Mizutani et al., 2004) with AlexaFluor 568 anti-rabbit IgG or anti-rabbit IgG-HRP (Thermo Fisher) by indirect immunofluorescence or immunoblot analyses as previously reported (Ohashi et al., 2018).

Cell viability and virus induced cytopathology. Cell viability was determined by MTT assay as previously reported (Ohashi et al., 2018). Virus-induced cytopathology was observed by microscopy at 48 h post-infection as previously reported (Matsuyama et al., 2020).

Chemical screening. We screened an FDA/EMA/PMDA-approved chemical library composed of 306 compounds. Cells were treated with compounds at 8, 16, or 30 μM for 1 h during virus inoculation and for up to 72 h post-inoculation. The cells were then fixed with 4% paraformaldehyde and stained with DAPI to count viable cells using a high-content imaging system (ImageXpress Micro Confocal, Molecular Devices). Compounds that protected cells from virus-induced cytopathology and showed survival cell number more than 20-fold of the control were selected as hits. The list of compounds used in this study is shown in Table S1. Among 306 tested compounds, Cepharanthine, Lopinavir, Loteprednol, Nelfinavir, and Rapamycin were selected as hits. Lopinavir is already underway for clinical trial as anti-SARS-CoV-2 agents (Cao et al., 2020). As Loteprednol and Rapamycin are steroid and immunosuppressant, respectively, we focused on Cepharanthine and Nelfinavir in this study.

Docking simulation of a target protein and a compound. The crystal structure of the main protease and spike protein were obtained from Protein Data Bank (6LU7 (Jin et al., 2020) and 6M0J (Lan et al., 2020)) and refined for docking simulations using the Protein Preparation Wizard Script within Maestro (Schrödinger, LLC). We carried out *in silico* library screening based on the active site pocket of the main protease using combined molecular docking with a protein-ligand interaction fingerprint scoring method against 8,085 known drugs obtained from the KEGG-Drug database (Kanehisa and Goto, 2000). For all compounds ionization and energy minimization were performed by the OPLS3 force field in the LigPrep Script of Maestro (Schrödinger, LLC). These minimized structures were used as input structures for docking simulations. Docking simulations were performed using the Glide (Friesner et al., 2004; Halgren et al., 2004) SP docking program (Schrödinger, LLC) with a grid box defined by N3 inhibitor molecule for main protease and ACE2 binding interface residues for spike protein using BioLuminate (Schrödinger, LLC)

Mathematical analysis. Determination of synergism between NFV and CEP and simulation of virus dynamics as well as the calculation of IIP are shown in Supplementary Note in detail.

Statistics. All experiments were repeated three times in each assay. Statistical significance estimated using the two-tailed Student's t test (*$p<0.05$; **$p<0.01$; N.S., not significant).

Supplementary Note

Quantifying instantaneous inhibitory potential (IIP) from the dose-response curves of the drugs

The typical dose-response curves of a single antiviral drug can be analyzed using the following Hill function (Koizumi et al., 2017) (**Fig. 1E**):

$$f_u = \frac{1}{1 + \left(\frac{D}{IC_{50}}\right)^m}. \qquad (1)$$

Here, f_u represents the fraction of infection events unaffected by the drug (i.e., $1 - f_u$ equals the fraction of drug-affected events). D is the drug concentration, IC_{50} is the drug concentration that achieves 50% inhibition of activity, and m is the slope of the dose-response curve (i.e., Hill coefficient) (Koizumi et al., 2017). Dose-response curves for drugs with higher m values show stronger antiviral activity at the same normalized drug concentration so long as the drug concentration is higher than IC_{50} (**Fig. 1E**). Least-square regression approach was used to fit Eq.(1) to dose-response data and estimate the values of IC_{50} and m. Those estimated values for each drug against SARS-CoV-2 are summarized in **Table S2**.

We evaluated the intrinsic antiviral activity of anti-SARS-CoV-2 agents (**Fig. 1G**). The antiviral activity of antiviral drugs can be expressed as the instantaneous inhibitory potential (IIP) (Jilek et al., 2012; Laskey and Siliciano, 2014; Sampah et al., 2011; Shen et al., 2008; Shen et al., 2011; Shen et al., 2009):

$$\mathrm{IIP} = \log\left(\frac{1}{f_u}\right) = \log\left[1 + \left(\frac{D}{IC_{50}}\right)^m\right]. \qquad (2)$$

If a drug reduces SARS-CoV-2 replication by 1 log then $f_u = 0.1$ and its $\mathrm{IIP} = 1$, whereas if it reduces replication by 2 logs, i.e. 100-fold, its $\mathrm{IIP} = 2$. Note that the IIP incorporates all three parameters of the dose-response curve; D, IC_{50} and m. Eq. (2) indicates that the higher the m of the drug, the higher the IIP at a given D and IC_{50}.

Expected anti-SARS-CoV-2 effect of double-drug combinations by Bliss independence

We evaluated the effect of double-drug combinations for Bliss independence which is widely used to analyze drug combination data (Bliss, 1939; Kobayashi et al., 2014; Koizumi and Iwami, 2014; Tallarida, 2001). Bliss independence assumes that each drug acts on different targets, and is defined as:

$$f_u^{\mathrm{Bcom}} = f_u^A(D) \times f_u^B(D), \qquad (3)$$

where f_u^{Bcom}, f_u^A and f_u^B are the fractions of infection events unaffected by the combined drugs A (i.e., Nelfinavir: NFV) and B (i.e., Cepharanthine: CEP) expected by the Bliss model, single drug A and single drug B defined by Eq. (1), respectively. Using Eq. (2), we expected the anti-SARS-CoV2 effects of combined drugs A and B, $1 - f_u^{\mathrm{Bcom}}$, from the anti-SARS-CoV-2 effects of the single drugs (**Fig. S1**).

However, the Bliss model ignores interactions in which drugs enhance each other effects. To address this point, we introduced the recent proposed model (Zimmer et al., 2016), called "dose model" considering the drug interactions, and further evaluated the expected antiviral effects (**Fig. S1**). This drug interaction is described by introducing interaction terms between drug pairs, that is, the "effective" concentration of drug A (i.e., NFV) and B (i.e., CEP), D_A^{com} and D_B^{com}, are defined as follows;

$$D_A^{\mathrm{com}} = D_A\left(1 + a_{AB}\frac{D_B^{\mathrm{com}}}{IC_{50}^B + D_B^{\mathrm{com}}}\right)^{-1}, \qquad D_B^{\mathrm{com}} = D_B\left(1 + a_{BA}\frac{D_A^{\mathrm{com}}}{IC_{50}^A + D_A^{\mathrm{com}}}\right)^{-1},$$

where D_A and D_B are the "true" concentrations, IC_{50}^A and IC_{50}^B are the concentrations that achieve 50% inhibition of activity, a_{AB} and a_{BA} are the interaction parameters for drug A and B, respectively. Note that IC_{50}^A and IC_{50}^B are corresponding to the estimations from the dose-response curves of a single antiviral drug in **Table S2**, and $a_{AB} = -0.462$ and $a_{BA} = 0.307$ are estimated from the dose-response curves of the double-drug combination. The dose model extended the Bliss model, thus, the expected anti-SARS-CoV-2 effect with effective concentration of drugs A and B (rather than the true concentrations) are calculated as $1 - f_u^{\mathrm{Dcom}}(D)$ and

$$f_u^{\mathrm{Dcom}} = f_u^A(D_A^{\mathrm{com}}) \times f_u^B(D_B^{\mathrm{com}}). \qquad (4)$$

The dose model assumed that the effects of drugs on each other's effective doses are multiplicative.

PK/PD/VD model for single- and double-drug combinations against SARS-CoV-2 infection

Based on a standard viral dynamics (VD) model (Ikeda et al., 2016), to describe COVID-19 dissemination among susceptible target cells, we used the following simple mathematical model proposed in (Kim et al., 2020):

$$\frac{df(t)}{dt} = -\beta f(t)V(t), \qquad (5)$$

$$\frac{dV(t)}{dt} = \gamma f(t)V(t) - \delta V(t), \qquad (6)$$

where $f(t)$ and $V(t)$ are the ratio of uninfected target cells and the amount of virus, respectively. The parameters β, γ, and δ represent the rate constant for virus infection, the maximum rate constant for viral replication and the death rate of infected cells, respectively. All viral load data including Singapore and Zhuhai patients (Young et al., 2020; Zou et al., 2020) were simultaneously fitted using a nonlinear mixed-effect modelling approach, which uses the whole samples to estimate population parameters while accounting for inter-individual variation. The estimated parameters and initial values used here are summarized in **Table S4**.

To investigate the expected outcome for anti-SARS-CoV-2 therapies with single-drug, we conducted *in silico* experiments with the following PK/PD/VD model for replication inhibitor such as Nelfinavir (**Fig. 4**);

$$\frac{df(t)}{dt} = -\beta f(t)V(t), \qquad (7)$$

$$\frac{dV(t)}{dt} = \big(1 - \varepsilon(t) \times H(t)\big)\gamma f(t)V(t) - \delta V(t), \qquad (8)$$

and for entry inhibitor such as Cepharanthine;

$$\frac{df(t)}{dt} = -\big(1-\eta(t)\times H(t)\big)\beta f(t)V(t), \qquad (9)$$

$$\frac{dV(t)}{dt} = \big(1-\eta(t)\times H(t)\big)\gamma f(t)V(t) - \delta V(t). \qquad (10)$$

Here $H(t)$ is a Heaviside step function defined as $H(t)=0$ if $t<T$: otherwise $H(t)=1$, where T is the initiation timing of the treatment, and the anti-SARS-CoV2 effect for $t>T$ are described as

$$\varepsilon(t)\ (\text{or}\ \eta(t)) = 1-f_u\big(D(t)\big) = 1-\frac{1}{1+\left(\frac{D(t)}{IC_{50}}\right)^m}, \qquad D(t)=C_{max}e^{-kt}$$

where C_{max} and k are the peak drug concentration and the elimination rate for corresponding drug, respectively. The parameter values for each drug used here are summarized in **Table S2**.

For anti-SARS-CoV-2 therapies with double-drug combinations, we extended as the following PK/PD/VD model assuming the dose model;

$$\frac{df(t)}{dt} = -\big(1-\eta(t)\times H(t)\big)\beta f(t)V(t), \qquad (11)$$

$$\frac{dV(t)}{dt} = \big(1-\varepsilon(t)\times H(t)\big)\big(1-\eta(t)\times H(t)\big)\gamma f(t)V(t) - \delta V(t). \qquad (12)$$

Here $H(t)$ is a Heaviside step function defined as $H(t)=0$ if $t<T$: otherwise $H(t)=1$, and the anti-SARS-CoV2 effect are described as

$$\varepsilon(t) = 1-f_u^A(D_A^{\text{com}}(t)\,) = 1-\frac{1}{1+\left(\frac{D_A^{\text{com}}(t)}{IC_{50}^A}\right)^{m_A}},$$

$$\eta(t) = 1-f_u^B\big(D_B^{\text{com}}(t)\big) = 1-\frac{1}{1+\left(\frac{D_B^{\text{com}}(t)}{IC_{50}^B}\right)^{m_B}},$$

$$D_A^{\text{com}}(t) = C_{\max}^A e^{-k_A t}\left(1+a_{AB}\frac{D_B^{\text{com}}(t)}{IC_{50}^B+D_B^{\text{com}}(t)}\right)^{-1},$$

$$D_B^{\text{com}}(t) = C_{\max}^B e^{-k_B t}\left(1+a_{BA}\frac{D_A^{\text{com}}(t)}{IC_{50}^A+D_A^{\text{com}}(t)}\right)^{-1}.$$

Note that we here evaluated the double-drug combination of NFV and CEP (**Fig. 4**), and the pharmacokinetics of NFV and CEP, $D_A^{\text{com}}(t)$ and $D_B^{\text{com}}(t)$, under the combination, are different from those, $D_A(t)$ and $D_B(t)$, under the single-drug treatment because of the effective drug concentration.

Evaluation of outcomes for anti-SARS-CoV-2 therapies

The antiviral effect of the anti-viral therapy on SARS-CoV-2 dynamics using Eqs. (7-12) and our estimated parameter values was calculated (**Fig. 4**). We evaluated the outcomes for the therapies defined as “period until virus elimination” and “reduction of cumulative virus production” (**Fig. S2**). Note

that the cumulative virus production, i.e., the area under the curve of viral load (AUC: $\int_0^{T_D} V(s)ds$), for SARS-CoV-2 was calculated, where T_D is the time for SARS-CoV-2 achieved the detection limit.

Supplementary Figure

Fig. S1.

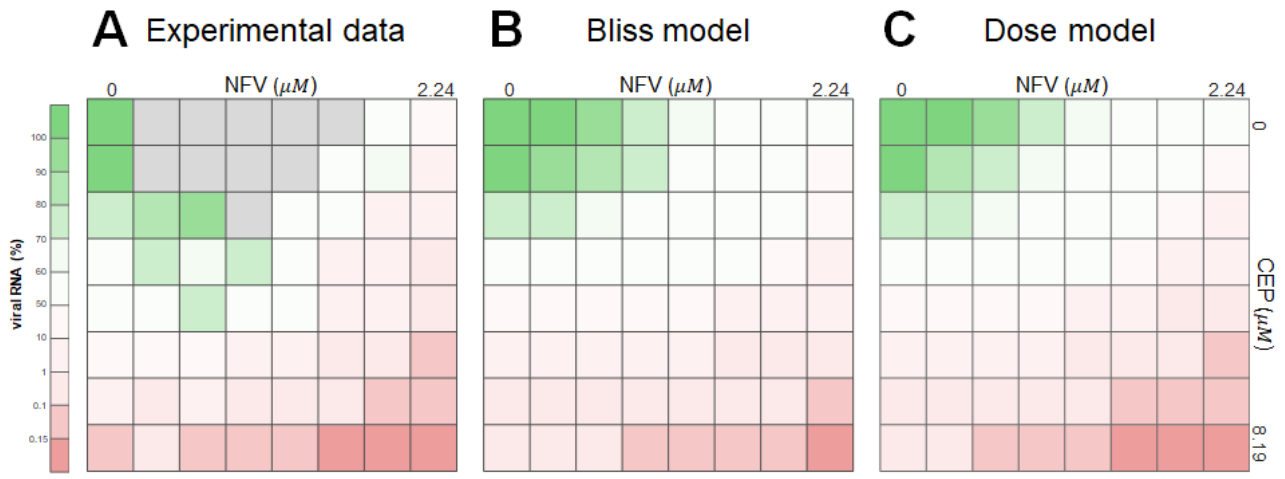

Fig. S1. Comparison of experimental data, Bliss model and Dose model for the double-drug combinations. Dose-response matrix of the double-drug combination (corresponding to **Fig. 3A**) are plotted in **(A)**, and the expected anti-SARS-CoV-2 effects of the double-drug combination (NFV and CEP) by the Bliss model and Dose model are plotted in **(B)** and **(C)**, respectively. Note that experimental measurements over 100% of viral RNA (implying large experimental variation because of small dose of antiviral drugs), colored by gray, were excluded in our analysis. The ratios of the values shown in **(A)** over those in **(B)** were calculated and are depicted in **Fig. 3C** in a 3D landscape.

Fig. S2.

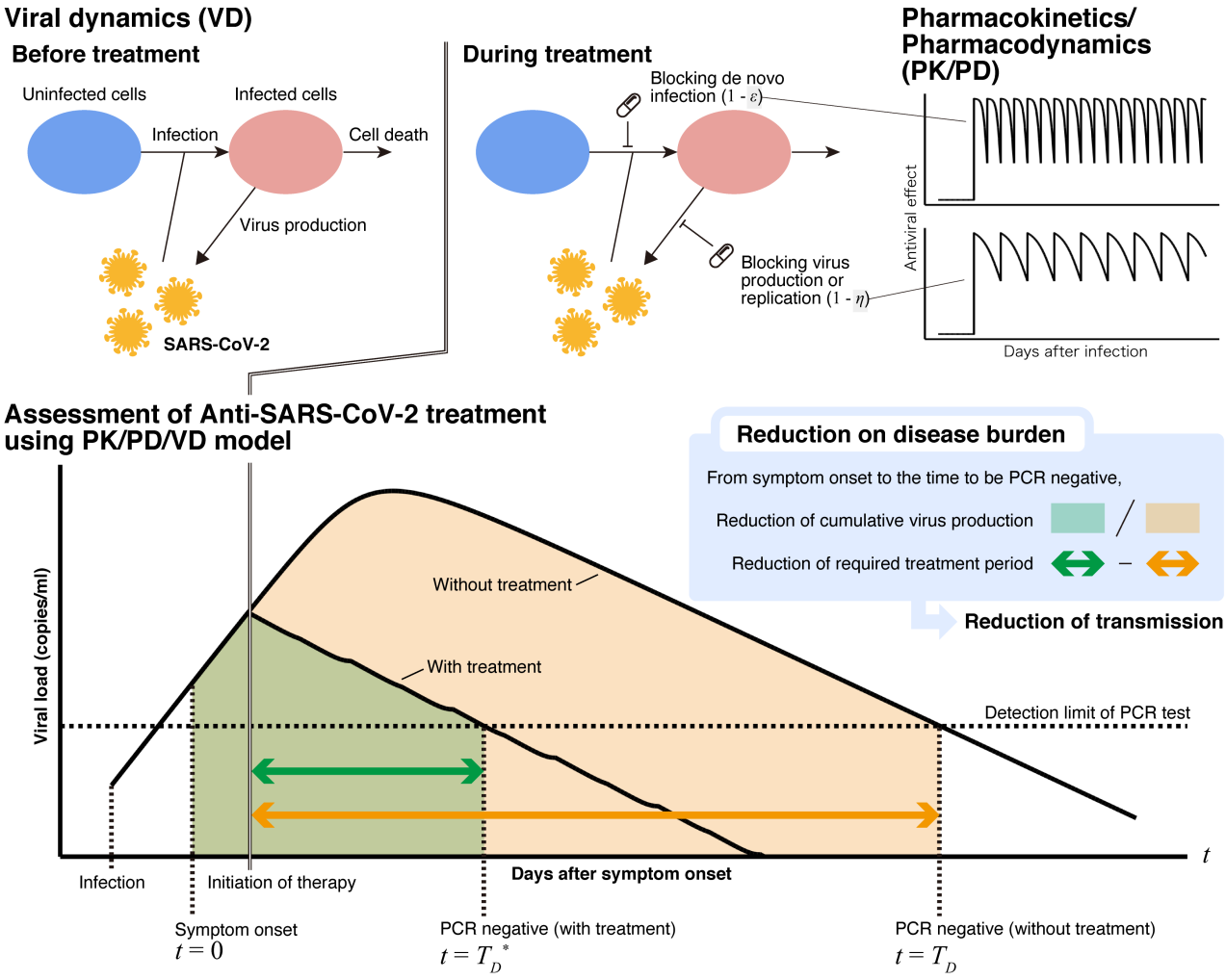

Fig. S2. Schematic representation of SARS-CoV-2 infection dynamics. A typical disease progress with viral load on patients undergoing therapy are shown. The outcomes for the therapies, that is, reduction in "period until virus elimination" and "cumulative virus production" are graphically depicted.

Supplementary Tables

Table S1. List of compounds in the screening

Abiraterone	Chlorprothixene	Favipiravir	Levodopa	Olopatadine	Rizatriptan
Acadesine	Cimetidine	Felodipine	Levofloxacin	Omega-3-Acid ethyl esters	Rosiglitazone
Acarbose	Clemastine fumarate	Fenbendazole	Levonorgestrel	Orlistat	Rutin
Acetohexamide	Clindamycin	Fenofibrate	Linagliptin	Oseltamivir	S-(+)-Rolipram
Acetylcysteine	clofibrate	Fidaxomicin	Lincomycin	Oxiconazole	Salbutamol sulfate
Acipimox	Clonidine	Fleroxacin	Lomustine	Oxybutynin	Simvastatin
Acitretin	Clotrimazole	Fluconazole	Loperamide	Oxymetazoline	Sodium butyrate
Acyclovir	Clozapine	Flucytosine	Lopinavir	Oxytetracycline	Sodium orthovanadate
Adapalene	Cortisone	Fluocinonide	Loteprednol	Ozagrel	Sorafenib
Adefovir Dipivoxil	Crystal violet	Flurbiprofen	Luliconazole	Paliperidone	Sotalol
Adenosine	Cytarabine	Fluvastatin	Manidipine	Pancuronium	Spectinomycin
Albendazole	Daclatasvir	Fudosteine	Maraviroc	Pazopanib HCl	Sulconazole
Alendronate	Daidzein	Furosemide	Masitinib	Pemafibrate	Sulfadiazine
Allopurinol	Dapoxetine	Gabapentin	Mesalamine	Pemetrexed	Sulfameter
Alogliptin	Dasatinib	Gadodiamide	Mesna	Phenylbutazone	Sulfamethoxazole
Amantadine	Deflazacort	Gallamine triethiodide	Mestranol	Pioglitazone	Sulfanilamide
Amenamevir	Delapril	Ganciclovir	Metformin	Piroxicam	Sulfisoxazole
Amfebutamone	Desonide	Gefitinib	Methenolone	Pitavastatin	Sulindac
Amiloride	Dexamethasone	Gemfibrozil	Methimazole	Potassium iodide	Tamoxifen
Aminocaproic acid	Dextran sulfate	Glazoprevir	Methocarbamol	Pramipexole	Taurine
5-aminolevulinic acid	Dextrose	Glecaprevir	Methoxsalen	Pravastatin	Telbivudine
Aminophylline	Diclofenac	Gliclazide	Methylprednisolone	Praziquantel	Telmisartan
Amlodipine besylate	Didanosine	Glimepiride	Metolazone	Prednisolone	Teneligliptin
Amorolfine	Dienogest	Glipizide	Micafungin	Prilocaine	Teniposide
Artemether	Diethylcarbamazine	Glyburide	Miconazole	Primidone	Terbinafine
Atazanavir	Difluprednate	glyclopyramide	Mifepristone	Progesterone	Terguride
Atovaquone	Diphenhydramine	Guaifenesin	Milrinone	Pyrazinamide	Testosterone
Atropine	Dipyridamole	Haloperidol	Mitiglinide	Pyridostigmine	Thioguanine
Baloxavir marboxil	Disulfiram	Hydrochlorothiazide	Mitoxantrone	Pyrimethamine	Tofogliflozin
Benazepril	Divalproex sodium	Hydrocortisone	Monobenzone	Quercetin	Toremifene Citrate
Benserazide	Dolutegravir	Hydroxyprogesterone	Moroxydine	Quetiapine fumarate	Torsemide
Betamethasone	Domperidone	Hydroxyurea	Mycophenolic	Quinine	Tranilast
Betapar	Donepezil	Ibuprofen	Naftopidil	Racecadotril	Trelagliptin
Bethanechol chloride	Drospirenone	Imatinib	Nateglinide	Raltegravir	Tretinoin
Bezafibrate	Elbasvir	Indapamide	Nefiracetam	Ramelteon	Triamcinolone
Bifonazole	Elvitegravir	Indomethacin	Nelfinavir	Ramipril	Trifluridine
Bortezomib	Empagliflozin	Ipragliflozin	Neostigmine	Ranitidine	Trilostane
Bupivacaine	Emtricitabine	Ipratropium bromide	Nevirapine	Ranolazine	Tropisetron
Busulfan	Enalapril	Isoconazole	Niacin	Rapamycin	Ursodiol
Canagliflozin	Entecavir	Isoniazid	Nicomol	Relugolix	Valganciclovir
Captopril	Eplerenone	Isoquercetin	Nicorandil	Repaglinide	Valsartan
Carbamazepine	Erlotinib	Ketoprofen	Nicotinamide	Reserpine	Vandetanib
Carbidopa	Erythromycin	Ketorolac	Nilotinib	retinyl acetate	Vardenafil
Cefdinir	Estradiol	L-Glutamine	Nimodipine	Ribavirin	Vicriviroc Malate
Cefditoren pivoxil	Estriol	Lamivudine	Nisoldipine	Rifabutin	Vidarabine
Cepharanthine	Estrone	Laninamivir	Nitazoxanide	Rifampicin	Vildagliptin
Chenodeoxycholic acid	Ethinyl estradiol	Lanoconazole	Nitrofurazone	Rifapentine	Vitamin b12
Chloramphenicol	Ethionamide	Lapatinib Ditosylate	Nizatidine	Rifaximin	Voglibose
Chlorothiazide	Ethyl Icosapentate	Lenalidomide	Novobiocin	Riluzole	Vorinostat
Chloroxine	Ezetimibe	Leuprorelin	Nystatin	Risperidone	Zalcitabine
Chlorpromazine	Famciclovir	Levamisole	Octreotide	Ritonavir	Zolmitriptan

Hit compounds shown in red

Table S2. Estimated characteristic parameters of the tested antiviral drugs

Drug (unit)	Class	IC_{50}	m
Lopinavir (μM)	RI	1.734	2.992
Nelfinavir (μM)	RI	1.317	4.043
Favipiravir (μM)	RI	4.057×10^{161}	5.610×10^{-3}
Chloroquine (μM)	EI	1.313	1.984
Cepharantine (μM)	EI	0.991	3.174

RI, replication inhibitor; EI, entry inhibitor

IC_{50}, 50% inhibitory concentration

m, slope of the dose-response curve (i.e., Hill coefficient)

Table S3. Summary of pharmacokinetic parameters of anti-SARS-CoV-2 drugs

Parameter name	Symbol	Unit	Nelfinavir	Cepharanthine	
				i.v.	p.o.
Single-compartment model					
Maximum concentration	C_{max}	μM	2.88	0.278	5.70×10^{-3}
Degradation rate	k	day^{-1}	4.89	0.268	2.45
Dosing schedule					
Initiation of treatment	t^*	day		0.500	
Dosing interval	τ	day	0.333	1.00	1.00

Nelfinavir: 500 mg, TID, orally

Cepharanthine: 100mg, intravenous injection (i.v.) or 120 mg, oral administration (p.o.)

Table S4. Estimated population parameters and initial values for SARS-CoV-2 infection

Parameter name	Symbol	Unit	Value
Maximum rate constant for viral replication	γ	day^{-1}	3.16
Rate constant for virus infection	β	$(copies/ml)^{-1}\ day^{-1}$	9.77×10^{-6}
Death rate of infected cells	δ	day^{-1}	0.165
Initial viral load	$V(0)$	copies/ml	5.64×10^{3}

Supplementary References

Bliss, C. (1939). The toxicity of poisons applied jointly1. Annals of applied biology. 26(3), 585-615.

Cao, B., Wang, Y., Wen, D., Liu, W., Wang, J., Fan, G., Ruan, L., Song, B., Cai, Y., Wei, M., et al. (2020). A Trial of Lopinavir-Ritonavir in Adults Hospitalized with Severe Covid-19. N Engl J Med. Published online 2020/03/19 DOI: 10.1056/NEJMoa2001282.

Corman, V.M., Landt, O., Kaiser, M., Molenkamp, R., Meijer, A., Chu, D.K.W., Bleicker, T., Brunink, S., Schneider, J., Schmidt, M.L., et al. (2020). Detection of 2019 novel coronavirus (2019-nCoV) by real-time RT-PCR. Euro Surveill. 25(3). Published online 2020/01/30 DOI: 10.2807/1560-7917.ES.2020.25.3.2000045.

Friesner, R.A., Banks, J.L., Murphy, R.B., Halgren, T.A., Klicic, J.J., Mainz, D.T., Repasky, M.P., Knoll, E.H., Shelley, M., Perry, J.K., et al. (2004). Glide: a new approach for rapid, accurate docking and scoring. 1. Method and assessment of docking accuracy. J Med Chem. 47(7), 1739-1749. Published online 2004/03/19 DOI: 10.1021/jm0306430.

Halgren, T.A., Murphy, R.B., Friesner, R.A., Beard, H.S., Frye, L.L., Pollard, W.T., and Banks, J.L. (2004). Glide: a new approach for rapid, accurate docking and scoring. 2. Enrichment factors in database screening. J Med Chem. 47(7), 1750-1759. Published online 2004/03/19 DOI: 10.1021/jm030644s.

Ikeda, H., Nakaoka, S., de Boer, R.J., Morita, S., Misawa, N., Koyanagi, Y., Aihara, K., Sato, K., and Iwami, S. (2016). Quantifying the effect of Vpu on the promotion of HIV-1 replication in the humanized mouse model. Retrovirology. 13, 23. Published online 2016/04/19 DOI: 10.1186/s12977-016-0252-2.

Jilek, B.L., Zarr, M., Sampah, M.E., Rabi, S.A., Bullen, C.K., Lai, J., Shen, L., and Siliciano, R.F. (2012). A quantitative basis for antiretroviral therapy for HIV-1 infection. Nature medicine. 18(3), 446-451. Published online 2012/02/22 DOI: 10.1038/nm.2649.

Jin, Z., Du, X., Xu, Y., Deng, Y., Liu, M., Zhao, Y., Zhang, B., Li, X., Zhang, L., Peng, C., et al. (2020). Structure of M(pro) from COVID-19 virus and discovery of its inhibitors. Nature. Published online 2020/04/10 DOI: 10.1038/s41586-020-2223-y.

Kanehisa, M., and Goto, S. (2000). KEGG: kyoto encyclopedia of genes and genomes. Nucleic Acids Res. 28(1), 27-30. Published online 1999/12/11 DOI: 10.1093/nar/28.1.27.

Kim, K.S., Ejima, K., Ito, Y., Iwanami, S., Ohashi, H., Koizumi, Y., Asai, Y., Nakaoka, S., Watashi, K., Thompson, R.N., et al. (2020). Modelling SARS-CoV-2 Dynamics: Implications for Therapy. medRxiv. 2020.2003.2023.20040493. DOI: 10.1101/2020.03.23.20040493.

Kobayashi, T., Koizumi, Y., Takeuchi, J.S., Misawa, N., Kimura, Y., Morita, S., Aihara, K., Koyanagi, Y., Iwami, S., and Sato, K. (2014). Quantification of deaminase activity-dependent and -independent restriction of HIV-1 replication mediated by APOBEC3F and APOBEC3G through experimental-mathematical investigation. J Virol. 88(10), 5881-5887. Published online 2014/03/14 DOI: 10.1128/jvi.00062-14.

Koizumi, Y., and Iwami, S. (2014). Mathematical modeling of multi-drugs therapy: a challenge for determining the optimal combinations of antiviral drugs. Theor Biol Med Model. 11, 41. Published online 2014/09/26 DOI: 10.1186/1742-4682-11-41.

Koizumi, Y., Ohashi, H., Nakajima, S., Tanaka, Y., Wakita, T., Perelson, A.S., Iwami, S., and Watashi, K. (2017). Quantifying antiviral activity optimizes drug combinations against hepatitis C virus infection. Proc Natl Acad Sci U S A. 114(8), 1922-1927. Published online 2017/02/09 DOI: 10.1073/pnas.1610197114.

Lan, J., Ge, J., Yu, J., Shan, S., Zhou, H., Fan, S., Zhang, Q., Shi, X., Wang, Q., Zhang, L., et al. (2020). Structure of the SARS-CoV-2 spike receptor-binding domain bound to the ACE2 receptor. Nature. Published online 2020/04/01 DOI: 10.1038/s41586-020-2180-5.

Laskey, S.B., and Siliciano, R.F. (2014). A mechanistic theory to explain the efficacy of antiretroviral therapy. Nat Rev Microbiol. 12(11), 772-780. Published online 2014/09/30 DOI: 10.1038/nrmicro3351.

Matsuyama, S., Nao, N., Shirato, K., Kawase, M., Saito, S., Takayama, I., Nagata, N., Sekizuka, T., Katoh, H., Kato, F., et al. (2020). Enhanced isolation of SARS-CoV-2 by TMPRSS2-expressing cells. Proc Natl Acad Sci U S A. 117(13), 7001-7003. Published online 2020/03/14 DOI: 10.1073/pnas.2002589117.

Mizutani, T., Fukushi, S., Saijo, M., Kurane, I., and Morikawa, S. (2004). Phosphorylation of p38 MAPK and its downstream targets in SARS coronavirus-infected cells. Biochem Biophys Res Commun. 319(4), 1228-1234. Published online 2004/06/15 DOI: 10.1016/j.bbrc.2004.05.107.

Ohashi, H., Nishioka, K., Nakajima, S., Kim, S., Suzuki, R., Aizaki, H., Fukasawa, M., Kamisuki, S., Sugawara, F., Ohtani, N., et al. (2018). The aryl hydrocarbon receptor-cytochrome P450 1A1 pathway controls lipid accumulation and enhances the permissiveness for hepatitis C virus assembly. J Biol Chem. 293(51), 19559-19571. Published online 2018/11/02 DOI: 10.1074/jbc.RA118.005033.

Sampah, M.E., Shen, L., Jilek, B.L., and Siliciano, R.F. (2011). Dose-response curve slope is a missing dimension in the analysis of HIV-1 drug resistance. Proc Natl Acad Sci U S A. 108(18), 7613-7618. Published online 2011/04/20 DOI: 10.1073/pnas.1018360108.

Shen, L., Peterson, S., Sedaghat, A.R., McMahon, M.A., Callender, M., Zhang, H., Zhou, Y., Pitt, E., Anderson, K.S., Acosta, E.P., et al. (2008). Dose-response curve slope sets class-specific limits on inhibitory potential of anti-HIV drugs. Nature medicine. 14(7), 762-766. Published online 2008/06/17 DOI: 10.1038/nm1777.

Shen, L., Rabi, S.A., Sedaghat, A.R., Shan, L., Lai, J., Xing, S., and Siliciano, R.F. (2011). A critical subset model provides a conceptual basis for the high antiviral activity of major HIV drugs. Sci Transl Med. 3(91), 91ra63. Published online 2011/07/15 DOI: 10.1126/scitranslmed.3002304.

Shen, L., Rabi, S.A., and Siliciano, R.F. (2009). A novel method for determining the inhibitory potential of anti-HIV drugs. Trends Pharmacol Sci. 30(12), 610-616. Published online 2009/10/20 DOI: 10.1016/j.tips.2009.09.003.

Tallarida, R.J. (2001). Drug synergism: its detection and applications. J Pharmacol Exp Ther. 298(3), 865-872. Published online 2001/08/16.

Wang, M., Cao, R., Zhang, L., Yang, X., Liu, J., Xu, M., Shi, Z., Hu, Z., Zhong, W., and Xiao, G. (2020). Remdesivir and chloroquine effectively inhibit the recently emerged novel coronavirus (2019-nCoV) in vitro. Cell Res. 30(3), 269-271. Published online 2020/02/06 DOI: 10.1038/s41422-020-0282-0.

Young, B.E., Ong, S.W.X., Kalimuddin, S., Low, J.G., Tan, S.Y., Loh, J., Ng, O.T., Marimuthu, K., Ang, L.W., Mak, T.M., et al. (2020). Epidemiologic Features and Clinical Course of Patients Infected With SARS-CoV-2 in Singapore. Jama. Published online 2020/03/04 DOI: 10.1001/jama.2020.3204.

Zimmer, A., Katzir, I., Dekel, E., Mayo, A.E., and Alon, U. (2016). Prediction of multidimensional drug dose responses based on measurements of drug pairs. Proc Natl Acad Sci U S A. 113(37), 10442-10447. Published online 2016/08/27 DOI: 10.1073/pnas.1606301113.

Zou, L., Ruan, F., Huang, M., Liang, L., Huang, H., Hong, Z., Yu, J., Kang, M., Song, Y., Xia, J., et al. (2020). SARS-CoV-2 Viral Load in Upper Respiratory Specimens of Infected Patients. N Engl J Med. Published online 2020/02/20 DOI: 10.1056/NEJMc2001737.